Unitary transformation between Cartesian- and polar-pixellated screens

Luis Edgar Vicent[1,*] and Kurt Bernardo Wolf[2,3]

[1]*División de Física Aplicada, Centro de Invetigación Científica y Estudios Superiores de Ensenada, Km. 107 carretera Tijuana-Ensenada, Ensenada, Baja California, 22860 México*
[2]*Instituto de Ciencias Físicas, Universidad Nacional Autónoma de México, Av. Universidad s/n, Col. Chamilpa, Cuernavaca, Morelos, 62251 México*
[3]*E-mail: bwolf@fis.unam.mx*
**Corresponding author: levicent@gmail.com*

Received March 14, 2008; accepted May 20, 2008;
posted May 27, 2008 (Doc. ID 93863); published July 3, 2008

A unitary transformation between Cartesian and polar pixellations of finite two-dimensional images is obtained from the su(2) model for discrete and finite signals. This transformation analyzes the original image into its finite Cartesian "Laguerre–Kravchuk" modes (involving Wigner little-d functions) and synthesizes it back using a polar mode basis with the same set of mode coefficients. The polar basis is derived from the quantum angular momentum theory, and its modes are given by Clebsch–Gordan coefficients. © 2008 Optical Society of America

OCIS codes: 100.2000, 200.6046, 070.2465, 070.2025, 270.5585.

1. INTRODUCTION

We describe here the unitary transformation of a finite image—a two-dimensional array of N^2 complex numbers—between Cartesian and polar pixellations. In the first case the pixels are arranged in an $N\times N$ square screen while in the second the pixels in the screen are placed on concentric circles of integer radii $r \in \{0,1,\ldots,N-1\}$ with $2r+1$ equally spaced pixels at each radius as shown in Fig. 1. Both the Cartesian and the polar screens have N^2 data points, so no information will be lost when this transformation is unitary. Cartesian sensor arrays are common and mathematically easy to separate, so their treatment simplifies to one-dimensional Fourier or other analyses. Sensor arrays with polar pixellation are less common but may be useful to discern the angular characteristics of circular beams. Since squares and circles obviously do not fit, the unitary transformation of data between Cartesian and polar arrays is not *prima facie* evident; interpolation to geometrically close data points on two such screens, for instance, is not unitary and hence not reversible.

While many continuous optical and quantum systems can be separated in Cartesian and polar coordinates, this paper addresses the problem of separation of variables for two *discrete* coordinates, equally spaced and of finite range, which for brevity we will call *finite* coordinates. In Section 2 we recount the discretization process from continuous to finite oscillator models in one dimension, freely using the tools of quantum angular momentum theory for the spin group SU(2) of 2×2 unitary matrices; this group is generated by the Lie algebra su(2) of Pauli matrices [1]. One-dimensional finite signals are thus represented by N-vectors of spin $j=\frac{1}{2}(N-1)$. This model has been detailed before in [2–4], among others.

Two-dimensional $N\times N$ Cartesian screens are introduced in Section 3 by the direct product of two su(2) algebras, subject to the gyration between the discrete versions of Hermite–Gauss and Laguerre–Gauss modes [5]. The angular momentum theory is used in Section 4 to find another two bases for the N^2 two-dimensional array of points conforming to the properties expected from the polar separation of coordinates. The overlap between the two is determined in Section 5, providing the explicit form of the unitary transformation, which includes Wigner little-d functions and Clebsch–Gordan coefficients. In Section 6 we report some numerical experiments and offer some conclusions.

2. su(2) MODEL FOR FINITE SIGNALS

The points on the surface of a freely rotating sphere project harmonic motion as do the points on the phase space plane under evolution in a harmonic oscillator potential. However, these two classical systems differ under the rest of the transformations that can rigidly act on these two manifolds. On the sphere one has the three components of angular momentum that generate the spin group SU(2) while on the plane one has translations, and the aforesaid rotations, that generate the group ISO(2) of Euclidean motions. We can picture the two systems as the sphere tangent to the phase space plane in Fig. 2, and see that in the limit of a growing radius the former will contract to the latter. This picture remains true when the classical quantities are quantized as the observable spectra of self-adjoint operators that act on an appropriate Hilbert space of functions.

These considerations led us to the su(2) model for one-dimensional N-point finite systems: one postulates that the three observables (q,p,λ) of position q, momentum p, and a "3-projection" λ (displaced energy) are the spectra of

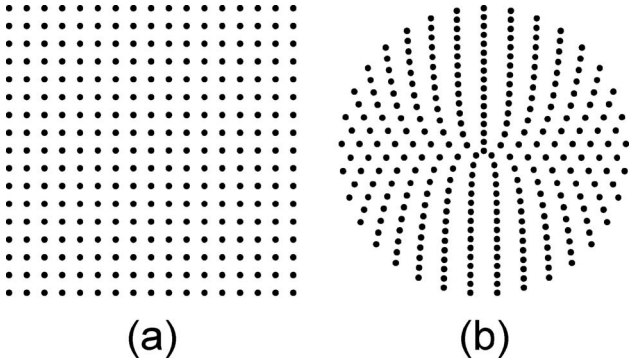

Fig. 1. (a) Cartesian and (b) polar arrangements of 17^2 pixel centers.

the three su(2) generators denoted by $\vec{J}=(J_1,J_2,J_3)$. These are abstractly characterized by their commutation relations $[J_i,J_j]=i\varepsilon_{i,j,k}J_k$ (i,j,k cyclic) that we can write as $\vec{J}\times\vec{J}=i\vec{J}$ and are realized as $N\times N$ self-adjoint matrices of a spin-j representation of su(2) for $N=2j+1$, a positive integer. The correspondence is [6]

$$\text{position: } Q=J_1, \tag{1}$$

$$\text{momentum: } P=J_2, \tag{2}$$

$$\text{3-projection: } L=J_3,$$

$$\text{mode number: } N=J_3+j1,$$

$$\text{energy: } H=J_3+\left(j+\tfrac{1}{2}\right)1. \tag{3}$$

The Hilbert space of signals is that of complex N vectors, where the spectrum of all three operators J_k is the finite point set $\{-j,-j+1,\ldots,j\}$. In this model therefore, positions and momenta are intrinsically finite, and there are

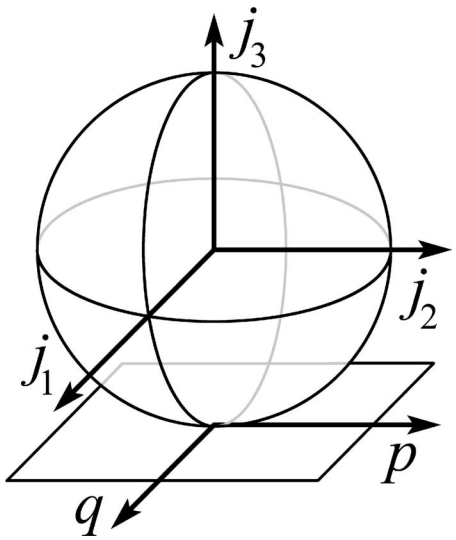

Fig. 2. Classical sphere with rotation axes j_1,j_2,j_3. Tangent to it, the phase space plane with translation directions q,p. The harmonic oscillator evolution rotates the figure around its vertical axis. We deform $q\to j_1, p\to j_2$, and identify the Hamiltonian with $h\to j_3+r$, where r is the radius of the sphere.

$2j+1$ energy eigenmodes numbered by $n:=\lambda+j\in\{0,1,\ldots,2j\}$.

The operator $H=N+\frac{1}{2}1=L+(j+\frac{1}{2})1$ is the finite oscillator Hamiltonian, whose commutation relations with position and momentum are

$$[H,Q]=iP,\quad [P,H]=iQ, \tag{4}$$

$$[Q,P]=iL=i\left(H-\left(j+\tfrac{1}{2}\right)1\right). \tag{5}$$

The first two equalities are the geometric and dynamic Hamilton equations for the harmonic oscillator (classical, quantum, or finite); the third commutator is the su(2) deformation of the familiar Heisenberg commutator of the usual Schrödinger operators in continuous systems. Finally, for spin j, the quadratic Casimir operator is represented by a multiple of the unit matrix

$$J^2:=Q^2+P^2+L^2=j(j+1)1. \tag{6}$$

We understand N-point signals $\mathbf{f}=\{f(q)\}_{q=-j}^{j}$ as the components of the vector $|\mathbf{f}\rangle$ in the orthonormal eigenbasis of the position operator in (1)

$$f(q):={}_1\langle j,q|\mathbf{f}\rangle,\quad \begin{cases} J^2|j,q\rangle_1=j(j+1)|j,q\rangle_1,\\ Q|j,q\rangle_1=q|j,q\rangle_1,\end{cases} \tag{7}$$

i.e., the Kronecker basis for N-point signals indicated by $|j,\cdot\rangle_1$. There is also the eigenbasis of the number operator N in Eq. (3); this basis is the set of N finite harmonic oscillator states $\Psi_n^{(N)}$ with $n|_0^{2j}$, $N=2j+1$. These we indicate by $|j,\lambda\rangle_3$ with $\lambda=n-j$ being its eigenvalue under L,

$$\begin{aligned}\Psi_n^{(N)}(q) &:= {}_1\langle j,q|j,\Lambda\rangle_3 \quad \begin{cases} J^2|j,\lambda\rangle_3=j(j+1)|j,\lambda\rangle_3,\\ L|j,\lambda\rangle_3=\lambda|j,\lambda\rangle_3.\end{cases}\\ &= d^j_{n-j,q}\left(\tfrac{1}{2}\pi\right),\end{aligned} \tag{8}$$

These are the matrix elements of a rotation around the j_2 axis of Fig. 2 that brings the j_3 axis onto the j_1 axis and are known as *little-d* Wigner functions [1],

$$d^j_{m,m'}(\beta)=d^j_{m',m}(-\beta)={}_3\langle j,m|\exp(-i\beta P)|j,m'\rangle_3, \tag{9}$$

for $\beta=\frac{1}{2}\pi$. The finite oscillator wave functions $\Psi_n^{(N)}(q)$ contain Gaussian hypergeometric ${}_2F_1$ functions and have the explicit form given by [1]

$$\begin{aligned} d^j_{m',m}(\beta)=&\frac{(-1)^{m-m'}}{(m'-m)!}\sqrt{\frac{(j-m)!\,(j+m')!}{(j+m)!\,(j-m')!}}\\ &\times\left(\cos\frac{1}{2}\beta\right)^{2j+m-m'}\left(\sin\frac{1}{2}\beta\right)^{m-m'}\\ &\times{}_2F_1\left(m'-j,-m-j;m'-m+1;-\tan^2\frac{1}{2}\beta\right).\end{aligned} \tag{10}$$

Additionally, the wave functions $\Psi_n^{(N)}(q)$ can be written in terms of the symmetric Kravchuk orthogonal polynomials [2,7–9]

$$\Psi_n^{(N)}(q) = d^j_{n-j,q}\left(\frac{1}{2}\pi\right) = \frac{(-1)^n}{2^j}\sqrt{\binom{2j}{n}\binom{2j}{j+q}}K_n\left(j+q;\frac{1}{2},2j\right), \quad (11)$$

where $\binom{x}{y}$ is the binomial coefficient defined for integer x and y—the factor $\binom{2j}{j+q}$ plays the role of a discrete Gaussian—and $K_n(x;p,N) := {}_2F_1(-n,-\frac{1}{2}N-x;-N;p^{-1})$ is the Kravchuk polynomial of degree n in x of parameter p [10]. The discrete oscillator wave functions $\Psi_n^{(N)}(q)$ in Eq. (11) are also called *Kravchuk functions*. In Fig. 3 we show the lower-, middle-, and highest-mode Kravchuk functions; this figure has appeared several times in literature, and a detailed study of their properties and symmetries can be found in [2,3,11].

A momentum eigenbasis of J_2 can be defined as in Eqs. (7) and (8), and the *Fourier–Kravchuk* transform [2], generated by the number operator in Eq. (3), rotates between these su(2) positions and momentum representations of the signal [12]. Finite coherent states that undergo harmonic motion are defined by any SU(2) transformation of the ground state $n=0$ in Eq. (8) using Eq. (9) for arbitrary β [11,13]. Finally, when $N\to\infty$ with the interval and density of points growing as $\sim\sqrt{N}$, one recovers the continuous harmonic oscillator algebra and wave functions [14]. This perfunctory construction of the su(2) model is all we need for the following sections.

3. TWO-DIMENSIONAL CARTESIAN SCREENS

The direct product (q_x,q_y) of two one-dimensional finite coordinates, each of N points, is a square $N\times N$ lattice of points, such as that in Fig. 1(a). On this point set we construct an $\mathrm{su}(2)_x\oplus\mathrm{su}(2)_y$ finite oscillator model, where the states of the system belong to the spin-(j,j) representation. The six generators are

$$Q_x,\ P_x,\ L_x = N_x - j1 = H_x - \left(j+\tfrac{1}{2}\right)1 \in \mathrm{su}(2)_x, \quad (12)$$

$$Q_y,\ P_y,\ L_y = N_y - j1 = H_y - \left(j+\tfrac{1}{2}\right)1 \in \mathrm{su}(2)_y. \quad (13)$$

The x generators and the y generators each obey the su(2) commutators in Eq. (5) and commute with each other; there are also the two quadratic Casimir operators J_x^2 and J_y^2 built as in Eq. (6). Following Eq. (8), the two-dimensional finite oscillator modes are the products

$$\Psi^{(N)}_{n_x,n_y}(q_x,q_y) = \Psi^{(N)}_{n_x}(q_x)\Psi^{(N)}_{n_y}(q_y) = d^j_{n_x-j,q_x}\left(\tfrac{1}{2}\pi\right)d^j_{n_y-j,q_y}\left(\tfrac{1}{2}\pi\right)$$
$$= {}_{1x}\langle j,q_x|j,n_x-j\rangle_{3x} \times {}_{1y}\langle j,q_y|j,n_y-j\rangle_{3y}$$
$$=: {}_1\langle j,q_x;j,q_y|j,n_x-j;j,n_y-j\rangle_3, \quad (14)$$

where $|j,q_x;j,q_y\rangle_1 = |j,q_x\rangle_{1x}|j,q_y\rangle_{1y}$ is the direct product of position eigenbases and similar to the mode number basis. As in Eq. (7), we regard an image on the Cartesian screen as a state $|\mathbf{F}\rangle$ whose components in the position basis $|j,q_x;j,q_y\rangle_1$ give its values in the corresponding pixel

$$F(q_x,q_y) = {}_1\langle j,q_x;j,q_y|\mathbf{F}\rangle. \quad (15)$$

We can organize the Cartesian states (n_x,n_y) into the rhombus pattern shown in Fig. 4; the rows are labeled by the total mode number $n=n_x+n_y$, $n|_0^{4j}$ and the columns by the energy difference $m=\frac{1}{2}(n_x-n_y)$; the latter are constrained into the rhombus by $|m|\le\frac{1}{2}n$ for $n\le 2j$, and $|m|\le 2j-1/2n$ for $n\ge 2j$. In Fig. 5 we show the two-dimensional finite oscillator Kravchuk functions in Eq. (14) placed in that rhombus pattern. These modes are the su(2) finite counterparts of the two-dimensional x–y separated Hermite–Gauss functions in continuum optics.

In the continuous two-dimensional models of quantum harmonic oscillators and of scalar waveguide optics, one builds the Poincaré sphere. On this sphere, Hermite–Gauss states are represented by points around the equator with an azimuth that is twice the angle of their separating coordinate frame; the two poles of the sphere represent Laguerre–Gauss beams with opposite angular momenta. The Poincaré sphere can be subject to rotations generated by operators of the second order in the Schrödinger operators of position and momentum, $\bar{Q}_k = q_k$ and $\bar{P}_k = -\mathrm{id}/\mathrm{d}q_k$ for $k=x,y$, which satisfy $[\bar{Q}_k,\bar{P}_{k'}]$

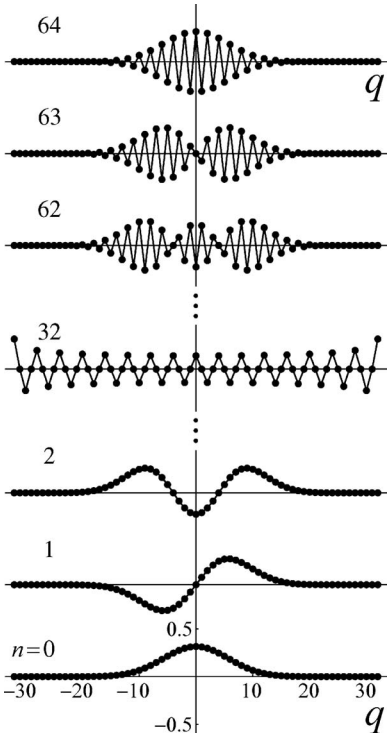

Fig. 3. Kravchuk functions, $\Psi_n^{(N)}(q)$ in Eq. (11), of the finite su(2) oscillator for $N=65$ $(j=32)$. Selected values of n show the lower, middle, and higher states. Note that the latter reproduce the former with alternating signs.

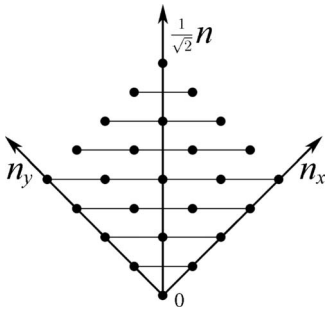

Fig. 4. Rhombus pattern for the two-dimensional finite oscillator states classified by the total mode number $n=n_x+n_y$.

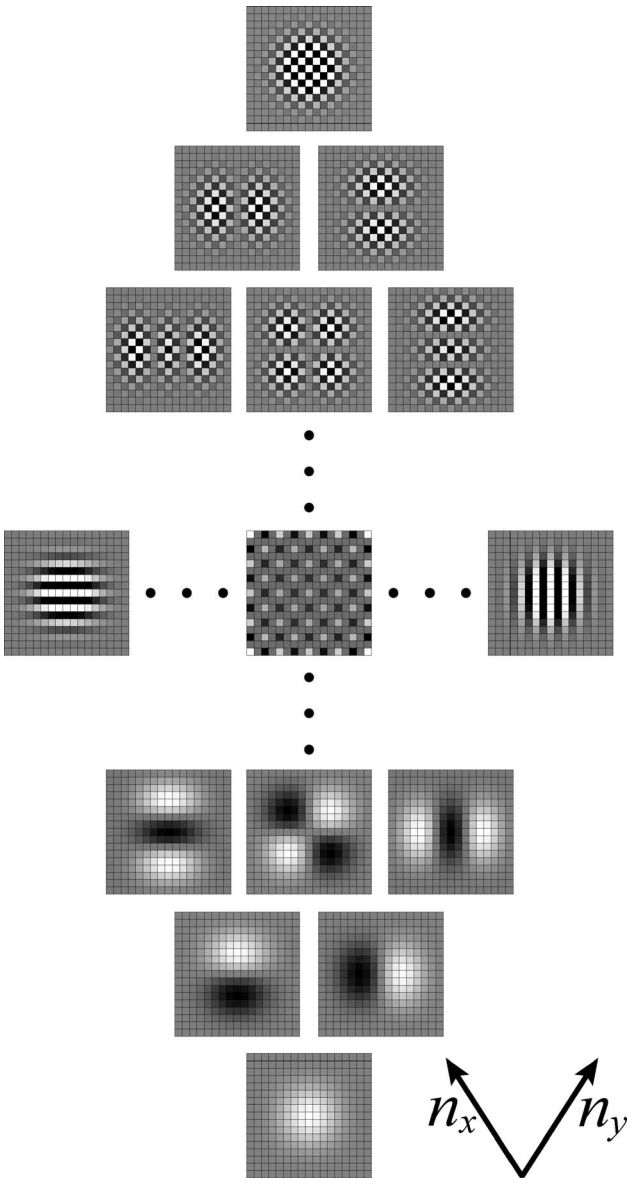

Fig. 5. Rhombus pattern of two-dimensional finite oscillator Kravchuk functions. The upper half of the rhombus reproduces the lower one with a checkerboard of alternating signs.

$=\delta_{k,k'}1$ [5,15]. This group of rotations is a subgroup of the group of all linear canonical transformations; since it contains the fractional Fourier transforms (FTs), it has been called the *Fourier* SU(2) group [16] and Subsection 10.3 of [17]. The three generators of this Fourier group, $\{F_k\}_{k=1}^3$, are identified as follows [5]:

$$\text{antisymmetric FT, } \bar{F}_1 := \tfrac{1}{4}(\bar{P}_x^2 - \bar{P}_y^2 + \bar{Q}_x^2 - \bar{Q}_y^2), \quad (16)$$

$$\text{gyration, } \bar{F}_2 := \tfrac{1}{2}(\bar{P}_x\bar{P}_y + \bar{Q}_x\bar{Q}_y), \quad (17)$$

$$\text{rotation, } \bar{F}_3 := \tfrac{1}{2}(\bar{Q}_x\bar{P}_y - \bar{Q}_y\bar{P}_x) =: \tfrac{1}{2}\bar{M}. \quad (18)$$

The commutation relations of these $\bar{F}_k$'s are $\vec{F}\times\vec{F}=\mathrm{i}\vec{F}$, the same as those of the J_k's in Section 2 and the same as any su(2) algebra. However the physical meaning of the two SU(2) groups is different: in Eq. (18), $\bar{M}=\bar{Q}\times\bar{P}$ is the physical orbital angular momentum operator; gyration, generated by Eq. (17), transforms Hermite–Gauss into Laguerre–Gauss beams; there is a fourth operator that commutes with the previous three, this is the

$$\text{symmetric FT, } \bar{F}_0 := \tfrac{1}{4}(\bar{P}_x^2 + \bar{P}_y^2 + \bar{Q}_x^2 + \bar{Q}_y^2 - 21). \quad (19)$$

The four generated transformations form the full *Fourier group* $\mathsf{U}(2)=\mathsf{U}(1)\otimes\mathsf{SU}(2)$ [16] and only transform beams among those with the same energy. The matrix representation of the gyration subgroup has elements given by Wigner *little-d* functions, as in Eq. (9), the same as in any SU(2) group.

Now we return to the finite two-dimensional model, noting that the generators of Eqs. (12) and (13) of $\mathsf{su}(2)_x \oplus \mathsf{su}(2)_y$ cannot be used to build a direct analog of the u(2) Fourier generators in Eqs. (16)–(19). Thus, one cannot produce in this way a finite analog of gyration that would conserve the energy of the x–y separated modes in Eq. (14), i.e., along the rows in Fig. 5 to find discrete "waveforms" with definite angular momentum as one does in the continuous case above. However, as shown in [5], one can *import* the transformation coefficients for gyration from the continuous model, indeed, from the abstract su(2) algebra, these coefficients are the Wigner little d's in Eqs. (8) and (9). The process of symmetry importation [18] yields here a unitary one-parameter group of linear transformation between all $n+1$ modes with the same total energy (mode number n, see Fig. 5). This is the discrete version of unitary gyration, which led in [5] to define Laguerre–Kravchuk modes on the $N\times N$ screen, $N=2j+1$, by

$$\Lambda_{n,m}^{(N)}(q_x,q_y) := \sum_{n_x+n_y=n} e^{\mathrm{i}\pi(n_x-n_y)/4} d^{n/2}_{1/2m,1/2(n_x-n_y)}\left(\tfrac{1}{2}\pi\right) \times \Psi^{(N)}_{n_x,n_y}(q_x,q_y), \quad (20)$$

$$n \in \{0,1,\ldots,4j\},$$

$$\begin{cases} n \le 2j & \Rightarrow \quad m \in \{-n,-n+2,\ldots,n\}, \\ n \ge 2j & \Rightarrow \quad m \in \{-4j+n,-4j+n+2,\ldots,4j-n\}. \end{cases} \quad (21)$$

As before, $N=2j+1$ is the number of pixels in each row or column of the Cartesian screen. In Fig. 6 we show these complex "angular momentum" modes using the same rhombus pattern in Fig. 5. The Laguerre–Kravchuk modes are orthonormal and complete in the N^2-dimensional space of complex functions supported on the points in Fig. 1(a).

In Fig. 6 we see that the behavior of the nodal lines (which separate positive from negative point values) for (n,m) in the lower half-rhombus supports the assignment of the integer quantum number m in Eqs. (20) and (21) and complies with properties expected from plane angular momentum states so that they are naturally arranged into spin-$\frac{1}{2}n$ multiplets; the number of radial nodal lines is $n-|m|$. Thus we adopt the Laguerre–Kravchuk functions in Eq. (20) as the optimal discrete analogs of the continuous Laguerre–Gauss functions characterized by

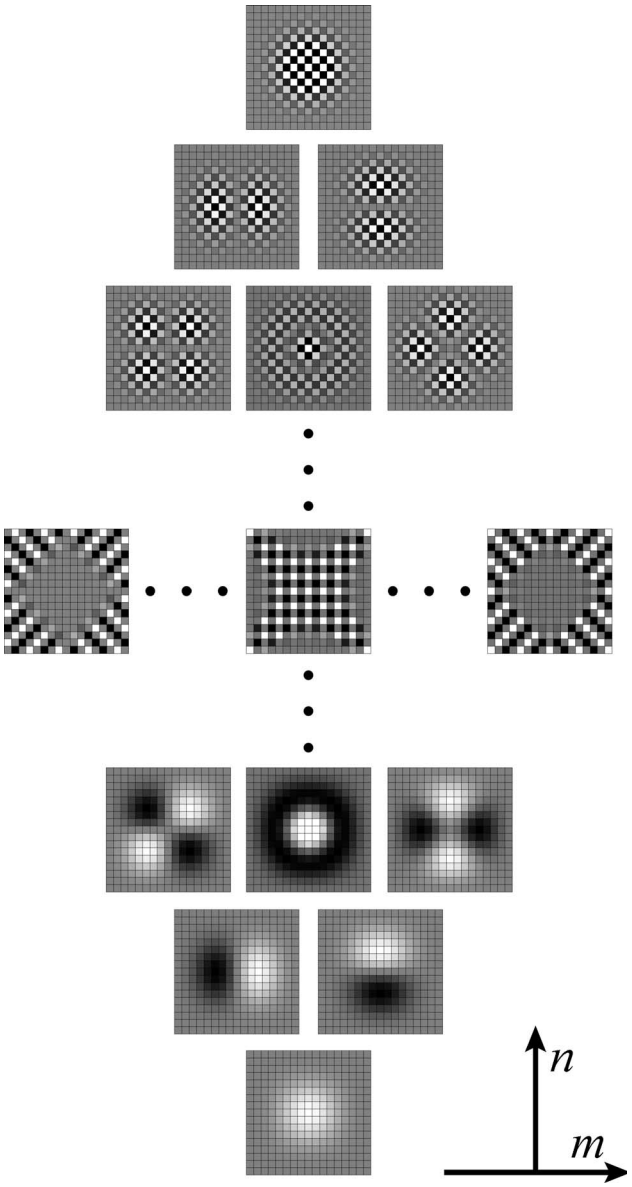

Fig. 6. Rhombus pattern of two-dimensional Laguerre–Kravchuk modes with definite angular momentum. Since the modes are complex, we plot the real modes $\Lambda^{(N),c}_{n,m}=\frac{1}{2}(\Lambda^{(N)}_{n,m}+\Lambda^{(N)}_{n,-m})$ for $m\geq 0$ on the right-hand side and $\Lambda^{(N),s}_{n,m}=-\frac{1}{2}\mathrm{i}(\Lambda^{(N)}_{n,m}-\Lambda^{(N)}_{n,-m})$ for $|m|>0$ on the left-hand side. The $m=0$ modes are real. Again, the upper triangle reproduces the lower one with a checkerboard of alternating signs.

the same quantum numbers. In Dirac notation we can indicate Eq. (20) for $N=2j+1$ by the ket

$$|j;n,m)_{\mathrm{LK}} := \sum_{n_x+n_y=n} e^{\mathrm{i}\pi(n_x-n_y)/4} d^{n/2}_{1/2m,1/2(n_x-n_y)}\left(\tfrac{1}{2}\pi\right) \times |j,n_x-j;j,n_y-j\rangle_3. \tag{22}$$

We use round brackets to indicate that one of its labels, angular momentum m, is *not* an eigenvalue under any operator in the algebra in Eqs. (12) and (13). On the other hand, the total mode number n does remain the eigenvalue of N_x+N_y while the two quadratic Casimir operators are $J_x^2=j(j+1)1=J_y^2$. These kets can be turned into wave functions by closing with the bra ${}_1\langle j,q_x;j,q_y|$. Finally, it should not escape attention that the linear combination coefficients in Eq. (22) are themselves Kravchuk functions given through Eq. (8) as

$$\Psi^{(n+1)}_{1/2(n+m)}\left(\tfrac{1}{2}(n_x-n_y)\right) = d^{n/2}_{1/2m,1/2(n_x-n_y)}\left(\tfrac{1}{2}\pi\right). \tag{23}$$

Although the Laguerre–Kravchuk states in Eq. (20) are all we need for the following sections, we should note that the imported gyration subgroup can be given for arbitrary angles γ essentially replacing the argument of the little-d function above by 2γ. This one-parameter group properly meshes with the "domestic" symmetric and antisymmetric Fourier–Kravchuk transforms whose eigenfunctions are in Eq. (14) with eigenvalues $n=n_x+n_y$ and $\frac{1}{2}(n_x-n_y)$. Thus we have the full Fourier group $\mathsf{U}(2)$ acting on finite systems, including the image rotation on the Cartesian grid, and its action is unitary [5].

4. TWO-DIMENSIONAL POLAR SCREENS

We used the algebra $\mathsf{su}(2)_x\oplus\mathsf{su}(2)_y$ in the (j,j) representation in Section 3, but now we will find two commuting operators whose eigenvalues can appropriately define a basis in that $(2j+1)^2$-dimensional space, by mode number and angular momentum (n,m), with the ranges in Eq. (21). Also, we should find two commuting operators whose eigenvalues have the meaning of radius and angle for the points to be arranged into a polar pattern as that in Fig. 1(b). Angle and angular momentum (with technical reservations) are canonically conjugate observables; in finite periodic signals they are determined by the Kronecker and Fourier bases, which are related to each other by the unitary finite FT matrix. Since there are k equidistant "angle" points on the circle supporting the signal, there will also be k angular momentum values in the Fourier basis.

Therefore, the two-dimensional problem is simplified to finding an operator that behaves as a radius (or *radius-squared*), namely, that it commutes with the chosen angular momentum generator. To place and name these operators it is convenient to look into the structure of the algebra generated by $\vec{J}_x=(Q_x,P_x,L_x)$ and $\vec{J}_y=(Q_y,P_y,L_y)$, writing linear combinations and their commutators as

$$\begin{matrix}\vec{J}_x\times\vec{J}_x=\mathrm{i}\vec{J}_x\\ \vec{J}_x\times\vec{J}_y=0\\ \vec{J}_y\times\vec{J}_y=\mathrm{i}\vec{J}_y\end{matrix}\quad\begin{matrix}\vec{J}_+:=\vec{J}_x+J_y\\ \vec{J}_-:=\vec{J}_x-J_y\end{matrix}\quad\Rightarrow\quad\begin{cases}\vec{J}_+\times\vec{J}_+=\mathrm{i}\vec{J}_+\\ \vec{J}_+\times\vec{J}_-=\mathrm{i}\vec{J}_-.\\ \vec{J}_-\times\vec{J}_-=\mathrm{i}\vec{J}_+\end{cases} \tag{24}$$

The six generators of the direct sum algebra $\mathsf{su}(2)_x\oplus\mathsf{su}(2)_y$ are thus separated into a subset of three J_+'s that close under commutation into the algebra denoted $\mathsf{su}(2)_+$ and three J_-'s that transform as a vector under this. Let us name the new component operators as follows:

$$\vec{J}_+ := \begin{pmatrix}R_+\\ S_+\\ L\end{pmatrix},\quad \vec{J}_- := \begin{pmatrix}-S_-\\ R_-\\ \frac{1}{2}M\end{pmatrix}, \tag{25}$$

where $L=L_x+L_y$ is the total 3-projection generator that provided the total energy or mode number $n=n_x+n_y$ in

Section 3 and $M=\frac{1}{2}(L_x-L_y)$ is the proposed finite angular momentum operator. The justification for this assignment of M is that it commutes with the total mode number, $[L,M]=0$ and that it generates joint rotations in the planes of (R_+,R_-) and of (S_+,S_-), namely,

$$[M,R_\pm]=\pm iR_\mp, \quad [M,S_\pm]=\pm iS_\mp. \tag{26}$$

In support of the proposition that $R_\pm$ and $S_\pm$ behave as position and momentum operators, we note that the total oscillator Hamiltonian $H:=N+1=L+(2j+1)1$ indeed generates joint rotations in the "phase space" planes (R_+,S_+) and (R_-,S_-) since

$$[L,R_\pm]=-iS_\pm, \quad [L,S_\pm]=iR_\mp. \tag{27}$$

From Eqs. (26) and (27), the choice of L and M to provide quantum mode and angular momentum eigenvalues (n,m) for finite polar kets seems appropriate. Regarding the "position and momentum" generators $R_\pm$ and $S_\pm$ we see that they also conform to the su(2) model since $[R_+,S_+]=iL=[R_-,S_-]$. However, the algebraic structure in Eq. (25) also fixes the commutators $[R_+,R_-]=iM=[S_+,S_-]$. These "nonstandard" commutators imply that the subset R_+,R_-,M (and also S_+,S_-,M) closes under commutation into an su(2) algebra that we distinguish by $\mathrm{su}(2)_\rho$; its quadratic Casimir operator

$$R^2:=R_+^2+R_-^2+M^2 \text{ commutes with } M. \tag{28}$$

This provides us with the radius-squared operator whose spectrum will be $\rho(\rho+1)$ with integer ρ ranging from 0 up to $2j$, as we will more fully argue below. The structure of $\mathrm{su}(2)_\rho$ also implies that the eigenvalues m of angular momentum M will range in $\{-\rho,-\rho+1,\ldots,\rho\}$. These $2\rho+1$ values determine that, after FT, the circles of radii ρ in Fig. 1(b) will have $2\rho+1$ points each so that the polar screen will consist of $\Sigma_{\rho=0}^{2j}(2\rho+1)=(2j+1)^2=N^2$ pixels, the same as the $N\times N$ Cartesian screen.

We thus have the following two bases for the $\mathrm{su}(2)_x\oplus\mathrm{su}(2)_y$ kets: that of total mode number $n=\lambda+j$, characterized by the eigenvalues λ under $L=J_{x3}+J_{y3}$ and m under $M=J_{x3}-J_{y3}$,

$$|j;\lambda,m\rangle_{\mathrm{L}},$$

$$\text{eigenkets of: } J_x^2 \quad J_y^2 \quad J_{x3} \quad J_{y3},$$

$$\text{eigenvalues: } j(j+1) \quad j(j+1) \quad \tfrac{1}{2}(\lambda+m) \quad \tfrac{1}{2}(\lambda-m), \tag{29}$$

and that of radius ρ and angular momentum m, characterized by

$$|j;\rho,m\rangle_{\mathrm{R}},$$

$$\text{eigenkets of: } (\vec{J}_x+\vec{J}_y)^2 \quad \vec{J}_x\cdot\vec{J}_y \quad R^2 \quad M,$$

$$\text{eigenvalues: } 2j(j+1) \quad 0 \quad \rho(\rho+1) \quad m. \tag{30}$$

To pass from the mode basis in Eq. (29) to the radius basis in Eq. (30) is, in angular momentum quantum mechanics, the coupling of two spin-j states to a sum of states of integer total spins $\rho\in\{0,1,\ldots,2j\}$ with *Clebsch–Gordan* (or su(2)-*Wigner*) coefficients, $C^{j,j,\rho}_{\cdots}$ as shown in Fig. 7.

The "third-component" eigenvalues in the Clebsch–Gordan coefficients must properly sum, yet we see that m in Eq. (30) is the *difference* of the eigenvalues of J_{3x} and J_{3y}; hence, a sign reversal of the latter is necessary before relating the overlap matrix of the two bases to *the* Clebsch–Gordan coefficients $C^{j,j,\rho}_{m_x,m_y,m}$, with $m_x+m_y=m$ [19]. Also, we should be aware that these coefficients were defined by recursion from their highest-m state, whereas the Kravchuk functions start from the ground state. Together, these two considerations relate the overlap of Eqs. (29) and (30) to the Clebsch–Gordan coefficients through a phase that must be carefully calculated [20]. The result is

$${}_{\mathrm{R}}\langle j;\rho,m|j;\lambda,m\rangle_{\mathrm{L}}=\varphi(j,\rho,\lambda,m)C^{j,j,\rho}_{1/2(m+\lambda),1/2(m-\lambda),m}, \tag{31}$$

with the phase

$$\varphi(j,\rho,\lambda,m)=(-1)^{j+\rho+1/2(|m|-m)}e^{i\pi\lambda/2}. \tag{32}$$

As we indicated at the beginning of this section, the $(2\rho+1)$-dimensional FT matrix will turn the kets $|j;\rho,m\rangle_{\mathrm{R}}$ into "angular" states that we denote by

$$|j;\rho,\theta_k)_{\mathrm{A}}:=\frac{1}{\sqrt{2\rho+1}}\sum_{m=-\rho}^{\rho}e^{-im\theta_k}|j;\rho,m\rangle_{\mathrm{R}}, \tag{33}$$

where k is an integer counted modulo $2\rho+1$ and the angles are $\theta_k=2\pi k/(2\rho+1)$ plus any function $c(\rho)$. This transformation is shown in Fig. 8, where we have aligned the $k=0$ points along a vertical ρ-axis by putting $c(\rho)=0$. Again, we have used round brackets in Eq. (33) to indicate that θ_k is *not* the eigenvalue of any operator built from the algebra but has been *imported*.

Thus we can finally write the basis of N^2 polar-separated finite functions, $N=2j+1$, by closing the mode-angular momentum kets $|j;n-j,m\rangle_{\mathrm{L}}$ in Eq. (29) with the bras in Eq. (33), and using Eq. (31) we find

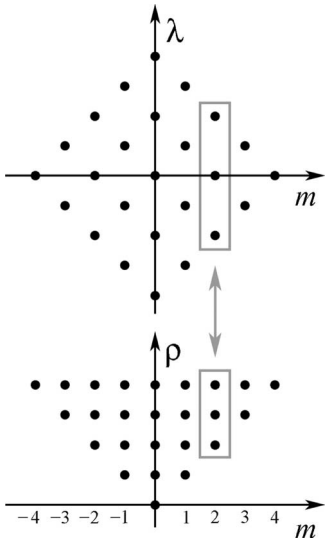

Fig. 7. States in the rhombus classified by mode number $n=j+\lambda$ and angular momentum m are related to states classified by radius ρ and the same angular momentum through Clebsch–Gordan coefficients.

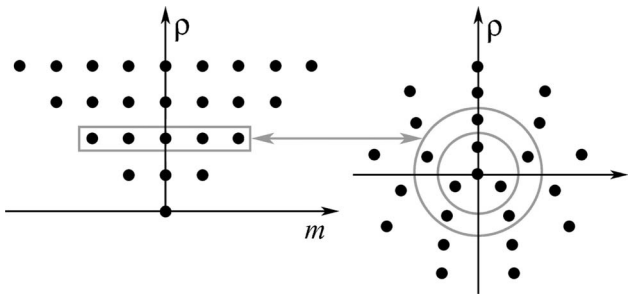

Fig. 8. States classified by radius ρ and angular momentum m are related, at each circle of radius ρ, to $2\rho+1$ kets associated with equally spaced points through the finite FT.

$$\Phi^{(N)}_{n,m}(\rho,\theta_k) \coloneqq {}_{\mathrm{A}}\langle j;\rho,\theta_k|j;n-j,m\rangle_{\mathrm{L}} = \frac{1}{\sqrt{2\rho+1}}\sum_{m=-\rho}^{\rho} e^{\mathrm{i}m\theta_k}\varphi(j,\rho,n-j,m) \times C^{j,j,\rho}_{1/2(m+n-j),1/2(m-n+j),m}. \tag{34}$$

The Clebsch–Gordan coefficients that contain the radius and angular momentum (ρ,m) are well known in the literature [1]; they can also be expressed as the product of a discrete function in ρ with the behavior of a decreasing exponential times a ${}_3F_2(\cdots|1)$ hypergeometric function, which for the appropriate negative integer values of the parameters is a discrete Hahn polynomial [21]. In the $N\to\infty$ limit, with radii decreasing as $\sim\rho/\sqrt{N}$, the radial part in Eq. (35) correctly contracts to the Laguerre functions of the two-dimensional quantum harmonic oscillator [22].

In Fig. 9 we show these "Laguerre–Kravchuk-on-polar-screen" functions, $\Phi^{(N)}_{n,m}(\rho,\theta_k)$ in Eq. (35), forming the same rhombus pattern for (n,m) as in Fig. 6 for the Cartesian (n,m) modes $\Lambda^{(N)}_{n,m}$ in Eq. (20). They are orthonormal and complete over the finite polar screen (ρ,θ_k). Since the Clebsch–Gordan coefficients include the restriction $|m|\le\rho$, the higher-m modes in Fig. 9 are only nonzero near to the edge of the screen for radii $|m|\le\rho\le 2j$. Properties noted for the Cartesian modes of Fig. 6, such as the sign alternation of the states in the upper triangle of the rhombus with respect to those in the lower one, also hold for the polar modes.

5. TRANSFER OF IMAGES

The basic proposition to unitarily transfer images from a square to a polar screen with the same number N^2 of points is to *identify* the (n,m) modes of the former in Fig. 6 with the corresponding (n,m) modes of the latter in Fig. 9. The modes in Eq. (14) are orthonormal and complete over the points of the Cartesian screen in Fig. 1(a) while the modes in Eq. (34) are over those of the polar screen in Fig. 1(b). Both sets of modes are orthonormal and complete over the *same* rhombus of points (n,m) in Fig. 4; the inner products in the first yield $\delta_{q_x,q_x'}\delta_{q_y,q_y'}$ while those of the second yield $\delta_{\rho,\rho'}\delta_{\theta_k,\theta_{k'}}$. The transformation between the Cartesian ket basis $|j,q_x;j,q_y\rangle_1$ in Eq. (14) and the polar ket basis $|j;\rho,\theta_k\rangle_{\mathrm{A}}$ in Eq. (33) is unitary because each of the transformations in Sections 3 and 4 have been unitary, both the domestic and the imported ones.

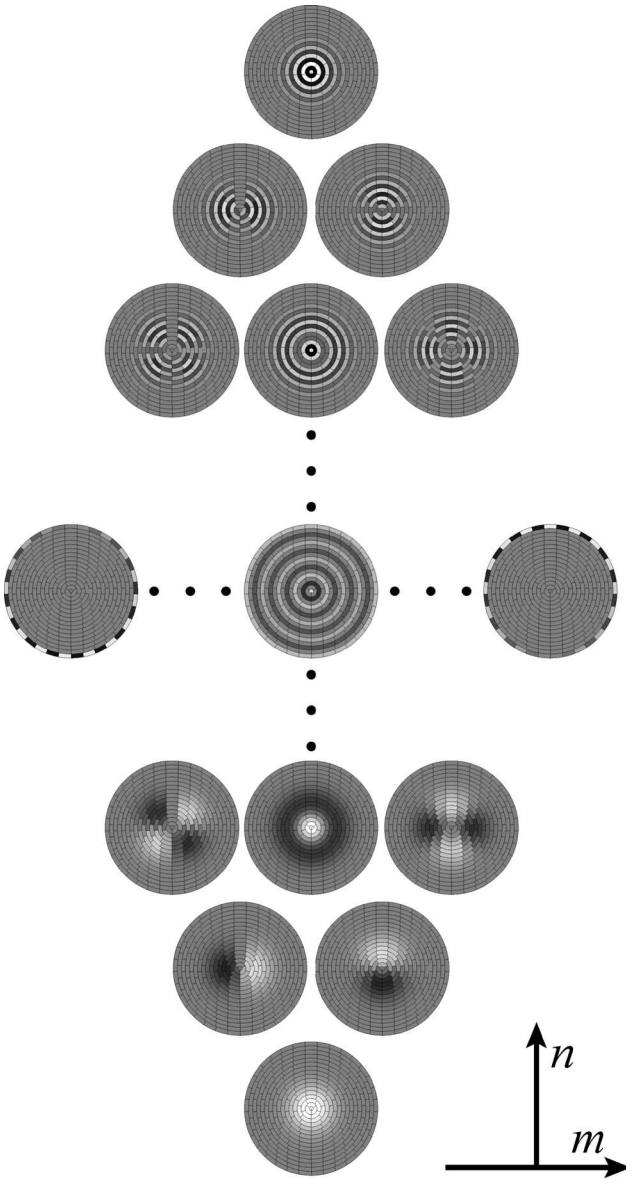

Fig. 9. Rhombus pattern of two-dimensional modes (n,m) with definite mode number and angular momentum on a screen with pixels that follow polar coordinates. Again, the modes are complex, so we show the real part of the modes for $m\ge 0$ on the right-hand side and the imaginary part for $|m|>0$ on the left-hand side. The functions are zero for radii $\rho<|m|$.

As in the one-dimensional case in Eq. (7), and on the two-dimensional Cartesian screen in Eq. (15), an N^2-point image on the polar screen $\mathbf{F}=\|F(\rho,\theta_k)\|$ is given by the set of components of $|\mathbf{F}\rangle$ in the position basis for $N=2j+1$,

$$F_\circ(\rho,\theta_k) \coloneqq {}_{\mathrm{A}}\langle j;\rho,\theta_k|\mathbf{F}\rangle \tag{35}$$

$$= \sum_{q_x,q_y=-j}^{j} {}_{\mathrm{A}}\langle j;\rho,\theta_k|j,q_x;j,q_y\rangle_1 \times {}_1\langle j,q_x;j,q_y|\mathbf{F}\rangle. \tag{36}$$

To relate the set of polar screen coefficients of the image to its Cartesian screen coefficients in Eq. (15), we need the overlaps of the position eigenbases. We use Eqs. (20)

and (34) to write this overlap as an $N^2\times N^2$ array of numerical coefficients,

$$U^{(N)}(\rho,\theta_k;q_x,q_y) \coloneqq {}_{\mathrm{A}}\langle j;\rho,\theta_k|j,q_x;j,q_y\rangle_1 = \sum_{n,m\in\Diamond} {}_{\mathrm{A}}\langle j;\rho,\theta_k|j;n-j,m\rangle_{\mathrm{L}} \times {}_{\mathrm{LK}}\langle j;n,m|j,q_x;j,q_y\rangle_1 \tag{37}$$

$$= \sum_{n,m\in\Diamond} \Phi^{(N)}_{n,m}(\rho,\theta_k)\Lambda^{(N)}_{n,m}(q_x,q_y)^*, \tag{38}$$

where $\Sigma_{n,m\in\Diamond}$ indicates the summation over the ranges specified in Eq. (21) of the polar $\Phi^{(N)}_{n,m}$ and Cartesian $\Lambda^{(N)}_{n,m}$ modes. Thus, the expansion in Eq. (35) is completed by

$$F_\circ(\rho,\theta_k) = \sum_{q_x,q_y=-j}^{j} U^{(N)}(\rho,\theta_k;q_x,q_y)F(q_x,q_y), \tag{39}$$

which relates the two sets of coordinates of *the same* vector $\mathbf{F}$ in the N^2-dimensional space of images. In the form of Eq. (38) it is easy to verify that this transformation is unitary, hence reversible, and given by

$$F(q_x,q_y) = \sum_{\rho,\theta_k\in\bigcirc} U^{(N)}(\rho,\theta_k;q_x,q_y)^* F_\circ(\rho,\theta_k), \tag{40}$$

where $\rho,\theta_k\in\bigcirc$ indicates the sum over $|k|\le\rho|_0^{2j}$.

6. DISCUSSION

We have defined Cartesian and polar "position" bases in the $(2j+1)^2$-dimensional space of two-dimensional finite images and found their overlap. The definitions were based on geometrical arguments, and the su(2) machinery was used to formalize the labels of mode number and angular momentum that were used to identify the images in Fig. 6 with those in Fig. 9. The calculation of the transformation kernel in Eq. (38) is algebraically arduous, so credible results should be computationally obtained to check and underline the theory. In Fig. 10 we generate a sharp and a soft "letter R" image (of 1's in a field of 0's) on a 65×65 Cartesian-pixellated screen and their transforms by Eq. (40) on a polar screen.

The Cartesian and polar renderings in Fig. 10 are very close if one discounts the appearance of zig-zags when sharp image edges do not conform with pixel coordinates; Gaussian smoothing of the images immediately reduces this effect. It is perhaps surprising that straight lines re-

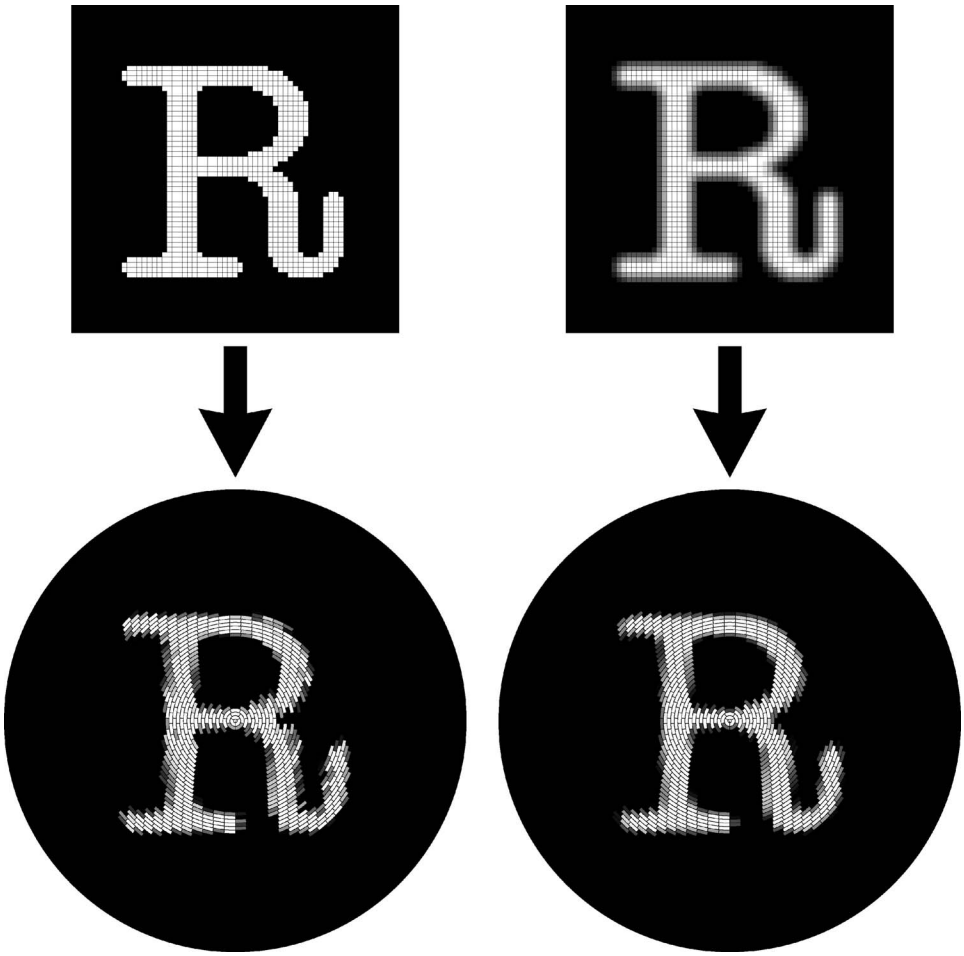

Fig. 10. Left: unitary map of a high-contrast image of 65^2 pixels from Cartesian (top) to polar (bottom) coordinates. Right: map of a low-contrast version. White corresponds to 1 and black to 0.

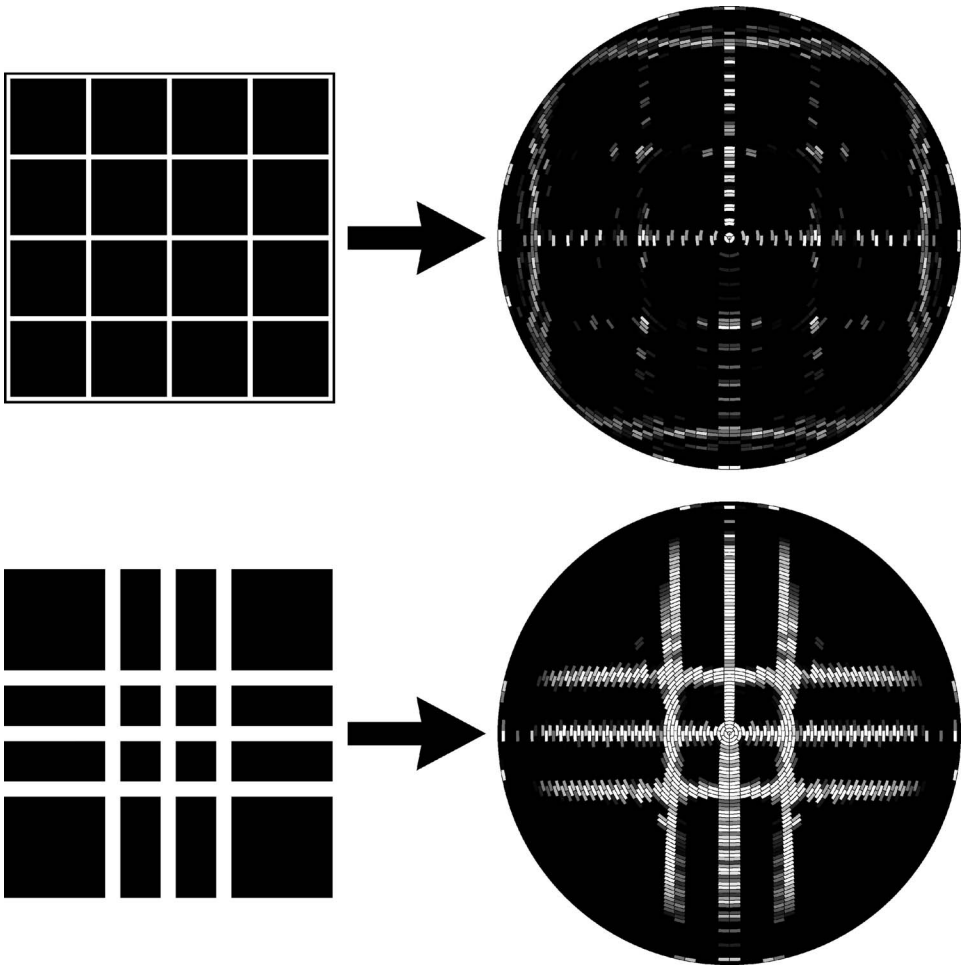

Fig. 11. Top: map of a square grid of one-pixel thick lines (in white). Bottom: map of a partial square grid of three-pixel thick lines (in white). As in Fig. 10, white corresponds to 1 and black to 0.

main visibly straight over the "R" in Fig. 10, which occupies about 2/3 of the linear size of the Cartesian image, or about half the area, as if the square were *inscribed* in the circle. To test which part of the Cartesian image is mapped into the parts of the circle out of this square, in Fig. 11 we map a square grid of one-pixel thick lines (of 1's on a field of 0's) and a partial square grid of three-pixel thick lines. The lines and vertices in the grid remain plainly visible, albeit distorted in the "no-fit" region between the square and the circle.

As we have shown, the transformation between images in the Cartesian- and polar-pixellated screens is an $N^2 \times N^2$ unitary matrix given by Eq. (38). This matrix can be reduced to a block-diagonal form based on its parity under reflections, which is common to both pixel configurations. The computational complexity of the Cartesian-to-polar transformation once the matrix elements of Eq. (38) have been numerically determined (as in all irreducible unitary transformations), grows as N^2 for one-dimensional N-point signals and N^4 for two-dimensional $N \times N$ images. This algorithm thus cannot be as fast as other *ad hoc* local interpolation algorithms nor can we bring to mind an optical setup to transform square into round images without loss of information. We hold in favor of our treatment that the transformation between square and round is well defined and has the proper continuum limits, properly meshes with the Fourier group, and is unitary, thus reversible.

We have separated discrete variables, exploiting the structure of the Lie algebra $\mathsf{su}(2)_x \oplus \mathsf{su}(2)_y$ in its (j,j)-representation, and reduced it with respect to two distinct subalgebra chains, one containing the Cartesian $\mathsf{u}(1)_x \oplus \mathsf{u}(1)_y$ and the other containing the polar $\mathsf{su}(2)_\rho \supset \mathsf{u}(1)_m$. Two extraneous unitary transformations (gyration and the FT) were imported onto the representation space and properly mesh into a $\mathsf{U}(2)$ Fourier group in Eqs. (16) and (17) that acts on the finite N^2-dimensional space of pixellated images.

Group theory provides the full classification of coordinates to separate the Hamiltonians through corresponding subalgebra chains and invariants [23]. Two dimensions are rather special in this and other respects (use of complex variables, etc.); for three dimensions the present construction leads to circular cylinder coordinates on the one hand and a Cartesian cube on the other. To both one may apply the Fourier group, which is $\mathsf{U}(3)$ there, containing the full rotation group of three-dimensional Cartesian-voxellated images.

ACKNOWLEDGMENTS

This work was performed under the support of project DGAPA-UNAM (Universidad Nacional Autónoma de

México) IN105008, *Óptica Matemática*. The authors thank Luis Mochán (Instituto de Ciencias Físicas, Universidad Nacional Autónoma de México) for the code in PEARL to graphically display the modes and figures in the polar screen.

REFERENCES

1. L. C. Biedenharn and J. D. Louck, "Angular momentum in quantum physics," in *Encyclopedia of Mathematics and Its Applications*, G.-C. Rota, ed. (Addison-Wesley, 1981), Vol. 8.
2. N. M. Atakishiyev and K. B. Wolf, "Fractional Fourier–Kravchuk transform," J. Opt. Soc. Am. A **14**, 1467–1477 (1997).
3. N. M. Atakishiyev, G. S. Pogosyan, L. E. Vicent, and K. B. Wolf, "Finite two-dimensional oscillator: I. The Cartesian model," J. Phys. A **34**, 9381–9398 (2001).
4. N. M. Atakishiyev, G. S. Pogosyan, L. E. Vicent, and K. B. Wolf, "Finite two-dimensional oscillator: II. The radial model," J. Phys. A **34**, 9399–9415 (2001).
5. T. Alieva and K. B. Wolf, "Rotation and gyration of finite two-dimensional modes," J. Opt. Soc. Am. A **25**, 365–370 (2008).
6. M. Arik, N. M. Atakishiyev, and K. B. Wolf, "Quantum algebraic structures compatible with the harmonic oscillator Newton equation," J. Phys. A **32**, L371–L376 (1999).
7. A. Erdélyi, W. Magnus, F. Oberhettinger, and F. G. Tricomi, *Higher Transcendental Functions* (McGraw-Hill, 1953), Vol. 2.
8. N. Ya. Vilenkin, *Special Functions and the Theory of Group Representations* (American Mathematical Society, 1968).
9. N. M. Atakishiyev and S. K. Suslov, "Difference analogs of the harmonic oscillator," Theor. Math. Phys. **85**, 1055–1062 (1991).
10. M. Krawtchouk, "Sur une généralization des polinômes d'Hermite," Acad. Sci., Paris, C. R. **189**, 620–622 (1929).
11. N. M. Atakishiyev, L. E. Vicent, and K. B. Wolf, "Continuous vs. discrete fractional Fourier transforms," J. Comput. Appl. Math. **107**, 73–95 (1999).
12. K. B. Wolf and G. Krötzsch, "Geometry and dynamics in the fractional discrete Fourier transform," J. Opt. Soc. Am. A **24**, 651–658 (2007).
13. L. E. Vicent, "Coherent states for the finite su(2)-oscillator model," Int. J. Mod. Phys. B **20**, 1934–1941 (2006).
14. N. M. Atakishiyev, G. S. Pogosyan, and K. B. Wolf, "Contraction of the finite one-dimensional oscillator," Int. J. Mod. Phys. A **18**, 317–327 (2003).
15. A. Frank and P. Van Isacker, *Algebraic Methods in Molecular and Nuclear Structure Physics* (Wiley, 1998).
16. R. Simon and K. B. Wolf, "Fractional Fourier transforms in two dimensions," J. Opt. Soc. Am. A **17**, 2368–2381 (2000).
17. K. B. Wolf, *Geometric Optics on Phase Space* (Springer-Verlag, 2004).
18. L. Barker, Ç. Çandan, T. Hakioğlu, M. A. Kutay, and H. M. Ozaktas, "The discrete harmonic oscillator, Harper's equation, and the discrete fractional Fourier transform," J. Phys. A **33**, 2209–2222 (2000).
19. R. Gilmore, *Lie Groups Lie Algebras and Some of Their Applications* (Wiley, 1974).
20. L. E. Vicent, "Análisis de Señales Discretas Finitas mediante el Modelo de Oscilador Finito de su(2)," Ph.D. dissertation (Universidad Autónoma del Estado de Morelos, 2007).
21. D. A. Varshalovich, A. N. Moskalev, and V. K. Khersonskiĭ, *Quantum Theory of Angular Momentum* (World Scientific, 1988).
22. N. M. Atakishiyev, G. S. Pogosyan, and K. B. Wolf, "Contraction of the finite radial oscillator," Int. J. Mod. Phys. A **18**, 329–341 (2003).
23. W. Miller, Jr., "Symmetry groups and separation of variables," in *Encyclopedia of Mathematics*, G.-C. Rota, ed. (Addison-Wesley, 1977), Vol. 4.